CHEMISTRY
A EUROPEAN JOURNAL

ChemPubSoc Europe

DOI: 10.1002/chem.201203673

Escherichia coli β-Galactosidase Inhibitors through Modifications at the Aglyconic Moiety: Experimental Evidence of Conformational Distortion in the Molecular Recognition Process

Luis Calle,[a] Virginia Roldós,[a] F. Javier Cañada,[a] María Laura Uhrig,[b] Alejandro J. Cagnoni,[b] Verónica E. Manzano,[b] Oscar Varela,[b] and Jesus Jiménez-Barbero*[a]

Abstract: Herein, we describe the use of thioglycosides as glycosidase inhibitors by employing novel modifications at the reducing end of these glycomimetics. The inhibitors display a basic galactopyranosyl unit (1→4)-bonded to a 3-deoxy-4-thiopentopyranose moiety. The molecular basis of the observed inhibition has been studied by using a combination of NMR spectroscopy and molecular modeling techniques. It is demonstrated that these molecules are not recognized by *Escherichia coli* β-galactosidase in their ground-state conformation, with a conformational selection process taking place. In fact, the observed conformational distortion depends on the chemical nature of the compounds and results from the rotation around the glycosidic linkage (variation of Φ or Ψ) or from the deformation of the six-membered ring of the pentopyranose. The bound conformations of the ligand are adapted in the enzymatic pocket with a variety of hydrogen-bond, van der Waals, and stacking interactions.

Keywords: conformation analysis · enzyme models · glycosides · NMR spectroscopy · S ligands

Introduction

There has been an intensive quest for glycosidase inhibitors for many years, because these molecules are relevant for understanding and controlling a variety of processes that are involved in carbohydrate-mediated essential biological events. In recent years, key advances in the understanding of the glycosidase inhibition mechanism at atomic resolution have been achieved, thus providing the cornerstone for rational structure-based drug design.[1] The importance of ligand distortion during the recognition process that ultimately leads to the catalytic cleavage of the glycosidic linkage has been recently established by using a variety of experimental and theoretical methods. Thus, it has been demonstrated[2] that different enzymes are able to recognize their substrates in high-energy conformations, and that, depending on the chemical nature of the substrate and on the particular enzyme, there are preferred "distorted" shapes[3] of the six-membered rings that can be accommodated at the catalytic sites. The data reported so far have shown that these distortions take place at the "nonreducing" moiety of the glycosidic linkage that will be cleaved during the process, thus permitting the proper orientation of the aglycone to leave the enzyme site with minimal energy loss.[4]

One of the paradigmatic glycosidase enzymes, the *Escherichia coli* β-galactosidase, has been extensively employed as a model, at different degrees of complexity, for many different scientific purposes.[5] The key aspects of the catalytic and recognition residues have been elucidated by using X-ray crystallography and site-directed mutagenesis.[1b,6] The enzymatic pocket of *E. coli* β-galactosidase is well characterized and located at a defined cavity of the existing triosephosphate isomerase (TIM)-barrel structure of one of its domains.[7] The nucleophile is glutamic acid Glu^{537}, although the glutamic acid Glu^{461} and tyrosine Tyr^{503} residues bound to the magnesium ion are also intimately involved in the catalysis. Two other tryptophan residues (Trp^{568} and Trp^{999}) determine the complementary interaction surface between the enzyme and the nonpolar faces of the carbohydrate ligands, through CH–π-stacking interactions, as frequently found in carbohydrate-binding proteins. Thus, Trp^{568} interacts with H-3, H-4, and H-5 of the nonreducing galactose residue, whereas Trp^{999} stacks with the properly oriented hydrogen atoms of the aglyconic moiety.[8]

Thus, as mentioned above, the catalysis process in glycosidases takes place with distortion of the substrate. Usually,

[a] L. Calle, Dr. V. Roldós, Prof. Dr. F. J. Cañada, Prof. Dr. J. Jiménez-Barbero
Chemical and Physical Biology
Centro de Investigationes Biològicas
CSIC, Ramiro de Maetzu 9, 28040 Madrid (Spain)
Fax: (+34) 915-360-432
E-mail: jjbarbero@cib.csic.es

[b] M. L. Uhrig, A. J. Cagnoni, V. E. Manzano, O. Varela
CIHIDECAR-CONICET, Departamento de Química Orgánica
Facultad de Ciencias Exactas y Naturales
Universidad de Buenos Aires, Pabellón 2
Ciudad Universitaria, 1428 Buenos Aires (Argentina)

Supporting information for this article is available on the WWW under http://dx.doi.org/10.1002/chem.201203673.

there is a significant deformation of the shape of the pyranose ring, passing from the typical $^4C_1$ chair to a half-chair or sofa conformations, depending on the chemical nature of the sugar involved.[9] With regard to *E. coli* β-galactosidase, we have previously employed lactose mimetics and showed that this enzyme also distorts the ground-state conformation by rotating the glycosidic Φ angle to adopt an *anti*-like geometry. According to NMR spectroscopic studies,[10] the adopted shape resembles that of the transition state, with the aglycone ready to depart from the catalytic site.

In this work, novel inhibitors are presented, which, strikingly, are not distorted at the nonreducing end, and therefore, they are not strictly transition-state mimics: benzyl 3-deoxy-4-*S*-(β-D-galactopyranosyl)-4-thio-β-D-*erythro*-pentopyranoside (**1**) and benzyl 3-deoxy-4-*S*-(β-D-galactopyranosyl)-4-thio-β-D-*threo*-pentopyranoside (**2**) (Figure 1).[11] As we report below, they behave as, respectively, moderate or strong inhibitors of *E. coli* β-galactosidase. Owing to their chemical nature, they can adopt a variety of conformations since the energy barrier for rotation around the glycosidic Φ angle is low enough, and the pentopyranose ring is sufficiently flexible to assume chair or skew-boat conformations. Therefore, thiodisaccharides **1** and **2** are good models to provide insight into the capacity of the enzyme to accommodate different distorted geometries. Also, since both molecules present rather different inhibition abilities, a structure–activity correlation might be evaluated.

Results and Discussion

Thiodisaccharides **1** and **2** have been synthesized by Michael addition of per-*O*-acetyl-1-thio-β-D-galactopyranose to a pentose-derived 3-en-2-one, followed by reduction and O-deacetylation.[11]

Standard enzymatic experiments showed rather different inhibition constant values for both thiodisaccharides towards *E. coli* β-galactosidase, although they only differ in the stereochemistry at C2 of the pentopyranose reducing end (referred to here as the aglyconic moiety). Thus, compound **1** showed a moderate noncompetitive inhibition ($K_i = 800$ μM), whereas **2** was a stronger competitive inhibitor of *o*-nitrophenyl β-D-galactopyranoside hydrolysis, with $K_i = 32$ μM. To rationalize the observed difference of more than one order of magnitude in their K_i values, it was essential to establish the bound-state conformation of each molecule to the enzyme. The first step in explaining this is to study the conformational behavior. We carried out extensive NMR spectroscopic studies on solutions of the inhibitors as well as computational energy mapping.

Conformational analysis: A standard coupling constant (*J*) analysis was performed to characterize the shape of the six-membered rings of thiodisaccharides **1** and **2** in water (Table 1). Their experimentally determined vicinal couplings were quantitatively compared to those calculated for the standard $^4C_1$ and $^1C_4$ chair conformations of the pyranose rings. The coupling constants were calculated according to the generalized Karplus equation proposed by Altona (as implemented in the MSpin program) for the optimized chairs. This comparison was also assessed by quantitative analysis of the intraring nuclear Overhauser effect (NOE) cross-peaks in the 2D NOESY spectra. A schematic view of the conformational equilibrium deduced for **1** and **2** is shown in Figure 1.

The observed *J*/NOE patterns for the galactopyranose residues in **1** and **2** in the free state indicated the unique pres-

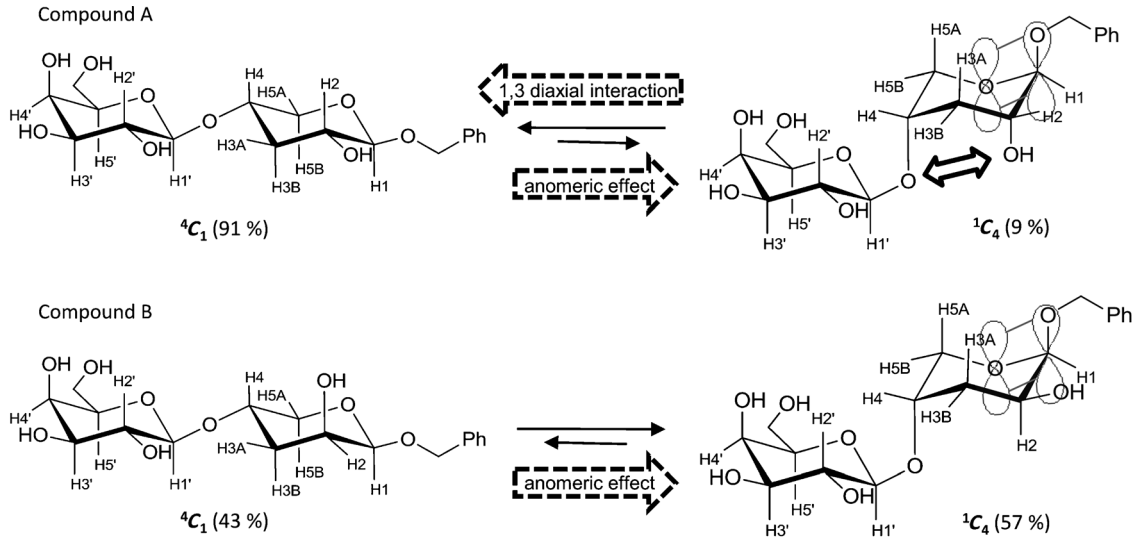

Figure 1. Conformation equilibrium for the pentopyranose ring of compounds **1** and **2** in solution. The populations were obtained by comparison of the experimental coupling constants with those estimated for the basic $^4C_1$ and $^1C_4$ geometries, calculated with the Karplus–Altona equation, as implemented in the MSpin program. The anomeric effect favors the $^1C_4$ conformation because the C1−O1 bond of the aglycone is axial with a C5-O5-C1-O1 torsion angle of 60° instead of equatorial (C5-O5-C1-O1 angle of 180°), the orientation found in the $^4C_1$ conformation.

Table 1. Experimental and calculated vicinal coupling constant values [Hz] for the chair conformations of the pentopyranose ring of **1** and **2**.

^3J(H,H)	**1** $^1C_4$ chair calcd	**1** $^4C_1$ chair calcd	**1** exptl	**2** $^1C_4$ chair calcd	**2** $^4C_1$ chair calcd	**2** exptl
H1,H2	2.0	6.5	7.4	3.1	0.9	2.6
H2[a],H3a	3.3	5.1	4.7	10.9	3.4	7.8
H2[a],H3b	2.7	10.7	10.7	4.8	2.9	4.1
H3a,H4	5.1	3.6	4.4	4.6	3.6	4.0
H3b,H4	1.9	11.9	10.8	2.1	11.9	8.7
H4,H5a	2.7	4.4	4.4	2.8	4.4	3.2
H4,H5b	1.0	11.3	11.4	1.0	11.3	5.7

[a] The stereochemistry at C2 is different for both compounds.

ence of the typical $^4C_1$ chair. In contrast, the pentopyranose rings of both **1** and **2** showed the presence of a conformational equilibrium between the two chair forms. Thus, in compound **1**, this ring mainly adopts the $^4C_1$ conformation (>90%) with a small population of the $^1C_4$ geometry (<10%). The free-energy difference between both conformers was calculated from the estimated populations to be approximately 1.4 kcal mol^{-1}. The existence of one very major conformer was also substantiated by the presence of a large long-distance coupling constant between H3eq and H5eq (^4J(H3eq,H5eq) = 2 Hz; Figure 2). This coupling suggests a W-type arrangement between the coupled protons, which only can take place for a well-defined shape, with no substantial conformational equilibrium. Alternatively, the ^{1}H NMR spectrum of **2** showed a distinct coupling pattern, and no long-range coupling constant was observed for H5a or H5b protons. The observed coupling constant values for the pentopyranose ring could be satisfactorily explained by an approximately 1:1 conformational equilibrium between the $^1C_4$ (53%) and $^4C_1$ (47%) chairs. This equilibrium precludes the observation of the long-range coupling (as in **1**).

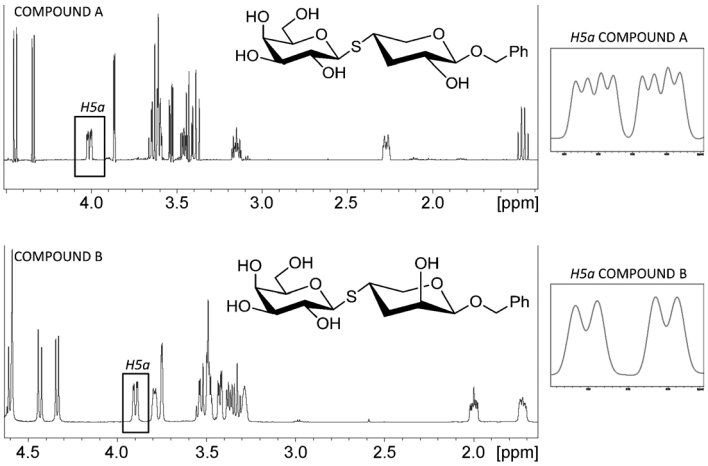

Figure 2. ^{1}H NMR spectra of thioglycosides **1** and **2**. In these structures, the pentopyranose ring has been depicted in the $^4C_1$ conformation. The inset on the right shows the H5a signal (equatorial in the $^4C_1$ and axial in the $^1C_4$ conformations; see Figure 1). In the case of **1**, the presence of a W-type long range coupling is only possible for H5a in the $^4C_1$ geometry of the pentose residue.

In spite of the expected preference for the $^1C_4$ pentopyranose chair for **1**, due to the anomeric effect, the $^4C_1$ conformer is the very major one. This shifting in the conformational equilibrium towards the $^4C_1$ chair is probably due to the existence of a 1,3-diaxial interaction between HO-2 of the deoxypentose (axial in the $^1C_4$ chair of **1**) and the interglycosydic sulfur atom. This is not the case for **2**, in which HO-2 is equatorial in the $^1C_4$ chair. The experimentally deduced populations might be employed to calculate the repulsive energy of the 1,3-O/S-diaxial interaction. The energy difference between the $^4C_1$ and $^1C_4$ conformations of **1** is approximately 1.4 kcal mol^{-1}, whereas for **2** it was calculated to be −0.1 kcal mol^{-1}. Therefore, the aforementioned 1,3-diaxial interaction ($\Delta\Delta G$) might be experimentally estimated as approximately 1.5 kcal mol^{-1}.

For the following step, the conformation around the thioglycosydic linkage was elucidated by a combined molecular mechanics/NMR spectroscopic approach. The torsion angles were defined as Φ = H1′-C1′-S-C4 and Ψ = C1′-S-C4-H4. Two different potential-energy maps were calculated for each molecule, with either the $^4C_1$ or the $^1C_4$ geometries at the aglyconic moiety (Figures S1–S3 in the Supporting Information). For both molecules, the calculations suggested the existence of three possible energy minima with the pentoses in the $^4C_1$ conformation (*syn*-$\Phi_{^4C_1}$/*syn*-$\Psi_{^4C_1}$, *anti*-$\Phi_{^4C_1}$/*syn*-$\Psi_{^4C_1}$, and *syn*-$\Phi_{^4C_1}$/*anti*-$\Psi_{^4C_1}$), and two other minima in which the pentopyranose moieties adopted the $^1C_4$ geometries (*syn*-$\Phi_{^1C_4}$/*syn*-$\Psi_{^1C_4}$ and *anti*-$\Phi_{^1C_4}$/*syn*-$\Psi_{^1C_4}$). Indeed, compounds **1** and **2** rendered very similar potential-energy maps for the glycosidic torsions, regardless of the configuration of the aglycone.

The presence of different Φ/Ψ conformations in the conformational distribution was confirmed by inspection of the interresidual NOEs (Figure 3). For **1**, the coupling-constant analysis had previously indicated (see above) that the $^4C_1$ chair of the aglyconic moiety was strongly predominant. Therefore, the population of the *syn*-$\Phi_{^1C_4}$/*syn*-$\Psi_{^1C_4}$ and *anti*-$\Phi_{^1C_4}$/*syn*-$\Psi_{^1C_4}$ forms would be very minor and difficult to deduce by NOE inspection. With regard to the other low-energy rotamers with the $^4C_1$ chair for the pentopyranose (*syn*-$\Phi_{^4C_1}$/*syn*-$\Psi_{^4C_1}$, *anti*-$\Phi_{^4C_1}$/*syn*-$\Psi_{^4C_1}$, and *syn*-$\Phi_{^4C_1}$/*anti*-$\Psi_{^4C_1}$), the presence of the *syn*-$\Phi_{^4C_1}$/*syn*-$\Psi_{^4C_1}$ was confirmed by the detection of two interresidual NOE contacts, available only to this conformation, between Gal H1′ and H4 of the aglyconic residue, and between Gal H1′ and H5a of the pentopyranose moiety. Additionally, the *syn*-$\Phi_{^4C_1}$/*anti*-$\Psi_{^4C_1}$ conformation was also identified due to the exclusive NOE contact between Gal H1′ and H3b of the aglycone. At this stage, the presence of the *anti*-$\Phi_{^4C_1}$/*syn*-$\Psi_{^4C_1}$ could not be detected in an unambiguous manner, since the key exclusive interresidual Gal H2′–H4 NOE overlapped with the expected H2–H4 intraresidual NOE within the pentopyranose ring in the $^4C_1$ chair. Thus, the population distribution contains two or three rotamers, always with the aglycone in the major $^4C_1$ chair.

The analysis of the NOEs for **2** (Figure 3) was even more complicated, since the *J* analysis had previously demonstrat-

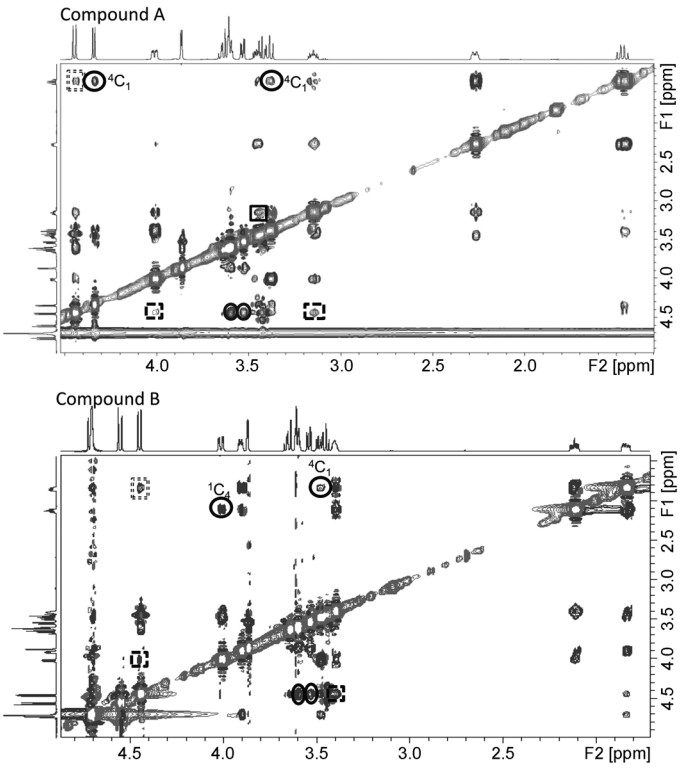

Figure 3. NOESY spectra in solution of both compounds (20 mM phosphate buffer with 1 mM $MgCl_2$ at pH 7.2 at 298 K). The circles highlight the characteristic NOE of chair conformations, and squares highlight the characteristic NOE of glycosidic torsion angles between galactose and aglyconic residue. Circles with legends refer to the aglyconic moiety, and circles without legends to those characteristic of the $^4C_1$ chair conformation of galactose residue. Dotted squares refer to *syn-Φ/anti-Ψ*, lined squares refer to *anti-Φ/syn-Ψ*, and complete squares refer to *syn-Φ/syn-Ψ*.

ed that the aglycone adopts two possible chair geometries. The existence of an NOE cross-peak between Gal H1′ and H4 of the aglyconic residue pointed out the presence of either $syn\text{-}\Phi_{^4C_1}/syn\text{-}\Psi_{^4C_1}$ or $syn\text{-}\Phi_{^1C_4}/syn\text{-}\Psi_{^1C_4}$ geometries, since this NOE is expected for both conformers. Nevertheless, the additional NOE between Gal H1′ and H5a is indicative of the presence of the $syn\text{-}\Phi_{^4C_1}/syn\text{-}\Psi_{^4C_1}$ form. The $syn\text{-}\Phi_{^1C_4}/syn\text{-}\Psi_{^1C_4}$ conformer could also exist, although it could not be confirmed by an NOE contact. The $syn\text{-}\Phi_{^4C_1}/anti\text{-}\Psi_{^4C_1}$ conformation could also be clearly detected by the existence of the exclusive NOE cross-peak between Gal H1′ and H3b of the pentopyranose. Again, the unambiguous presence of the $anti\text{-}\Phi_{^4C_1}/syn\text{-}\Psi_{^4C_1}$ and/or the $anti\text{-}\Phi_{^1C_4}/syn\text{-}\Psi_{^1C_4}$ could not be directly assessed due to overlapping of the exclusive cross-peak Gal H2′ and H4 of the aglycone with other intrarresidual ones. Therefore, a complex situation takes place for **2** in solution, with several conformers, from three to five, taking place in the conformational equilibrium.

The bound state: Insights into the structural and conformational features of the molecular recognition processes of both thiodisaccharides with *E. coli* β-galactosidase were obtained by employing the saturation transfer difference (STD)[12] and transferred (TR)-NOESY[13] experiments.

The enzyme–ligand interaction was evident from the STD analysis for different ligand/enzyme molar ratios, which also allowed us to determine the binding epitope of the interacting ligand. The data presented herein have been obtained for a ligand/enzyme 100:1 molar ratio, and the conclusions are basically identical to those obtained for other ratios. Strikingly, the STD-deduced epitope of **1** was somehow different from that of **2**. Indeed, for **1**, the largest STD percentages were observed for Gal H4′ and for the aromatic protons, whereas Gal H2′ and Gal H3′ received less saturation transfer than other aglyconic protons (Figure 4, top). In contrast, for **2**, there was a major transfer to the aromatic and the Gal protons, especially to Gal H2′, whereas the aglycone receives much less saturation from the protein (Figure 4, bottom). Then, as a control, STD experiments were also performed by employing the known inhibitor isopropyl 1-thiogalactopyranoside (IPTG). Interestingly, the STD pattern on the Gal hydrogen atoms of IPTG was basically identical to that found for **2** (Figure S4 in the Supporting Information). These experimental observations suggest that compounds **1** and **2** display different binding modes to the enzyme. We hypothesize that this could be one of the reasons for their different inhibition abilities.

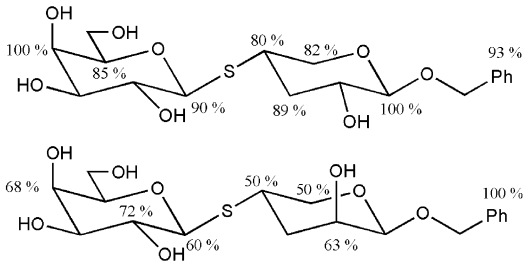

Figure 4. STD percentages measured for **1** (top) and **2** (bottom). Five saturation times between 0.5 and 2.5 s were used, with a protein/ligand 1:100 molar ratio in 20 mM phosphate buffer with 1 mM $MgCl_2$, at pH 7.2 and 298 K. The given numbers refer to the STD percentages at the longest saturation time. Only STD percentages of 50 % or higher are shown. For the methylene groups, the average of both protons are given. There are striking differences in the values for both compounds.

Additional information on the binding process was provided by TR-NOESY experiments, particularly with regard to the bound conformation of the two ligands in their complexes with β-galactosidase. As expected for the existence of a binding event, the NOE cross-peaks for the ligands in the presence of the enzyme (the ligand/enzyme molar ratio was now 30:1) were negative, in contrast with those observed in the free state (always positive, as expected for thiodisaccharides). In both cases, key differences in the pattern of many key NOE cross-peaks between the free and enzyme-bound states were found, which suggested that the bound conformations differed from those that are predominant in solution.

For bound thiodisaccharide **1**, characteristic NOE peaks (Figure 5) were detected that were consistent with the coexistence of both $^4C_1$ and $^1C_4$ chairs for the pentose unit. The

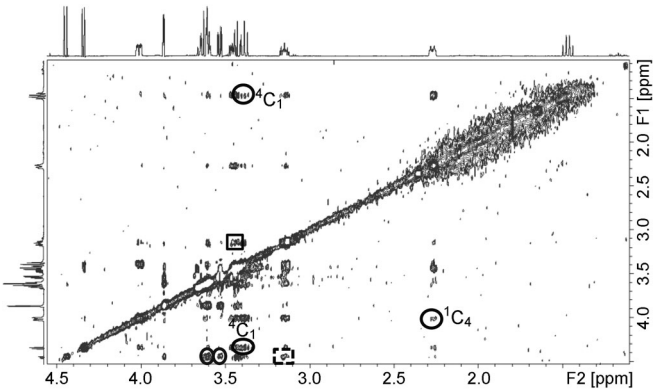

Figure 5. TR-NOESY of **1** (20 mM phosphate buffer with 1 mM $MgCl_2$ at pH 7.2 at 298 K). Circles highlight the key NOEs that define the different chair conformations of the aglycone, whereas the squares refer to the characteristic NOEs that define the conformations around the thioglycosydic torsion angles. Circles with legends refer to the aglyconic moiety, whereas the circles without legends refer to the Gal residue, which always presents a $^4C_1$ chair conformation. Lined squares indicate the presence of *anti*-$\Phi_{^4C_1}$/*syn*-$\Psi_{^4C_1}$ forms, whereas complete squares strongly suggest the existence of *syn*-$\Phi_{^1C_4}$/*syn*-$\Psi_{^1C_4}$ bound geometries, which were absent in the free state. Protein/ligand molar ratio was 1:30.

intrarresidual NOEs between H1 and H5b and between H3b and H5b denoted the presence of the $^4C_1$ chair of this residue. Simultaneously, the observed medium-sized NOE between H3a and H5a indicated the presence of the $^1C_4$ chair to a larger extent than that in the free state. Additionally, and also contrary to the free state, the absence of the exclusive interresidue NOE between H1′ and H3b in the TR-NOESY indicated that neither of the two possible *syn*-Φ/*anti*-Ψ conformations (with either $^1C_4$ or $^4C_1$ chair for the aglycone) was bound to the enzyme. On the other hand, the detection of an NOE between Gal H1′ and H4 of the aglycone confirmed the presence of *syn*-Φ/*syn*-Ψ forms, whereas the absence of H1′–H5a NOE contact excluded the *syn*-Φ/*syn*-Ψ with the $^4C_1$ chair as one of the binding conformers. *Anti*-Φ/*syn*-Ψ conformations could not be directly confirmed due to the overlapping between the aglycone H2 and Gal H2′, as already explained for the free state. The presence of conformers with the aglycone in the $^4C_1$ chair form indicated that these features should correspond to *anti*-$\Phi_{^4C_1}$/*syn*-$\Psi_{^4C_1}$ geometries around the glycosidic linkage. This bound conformation should coexist with the *syn*-$\Phi_{^1C_4}$/*syn*-$\Psi_{^1C_4}$ bound geometry, which was basically absent in the free state. Therefore, the ground-state conformation in a solution of **1** in water is not recognized by the enzyme, and two alternative high-energy conformations, *anti*-$\Phi_{^4C_1}$/*syn*-$\Psi_{^4C_1}$ and *syn*-$\Phi_{^1C_4}$/*syn*-$\Psi_{^1C_4}$, are bound. Therefore, the enzyme should provide interactions with the ligand that amount to at least 1.5–2 kcal mol^{-1} to bind these conformers.

A similar analysis of the TR-NOESY data was then performed for the complex between **2** and *E. coli* β-galactosidase. In this case, the data also suggested the binding of two different ligand shapes, which again corresponded with the *anti*-$\Phi_{^4C_1}$/*syn*-$\Psi_{^4C_1}$ and *syn*-$\Phi_{^1C_4}$/*syn*-$\Psi_{^1C_4}$ geometries (Figure 6). However, in this case, a distinct conformational

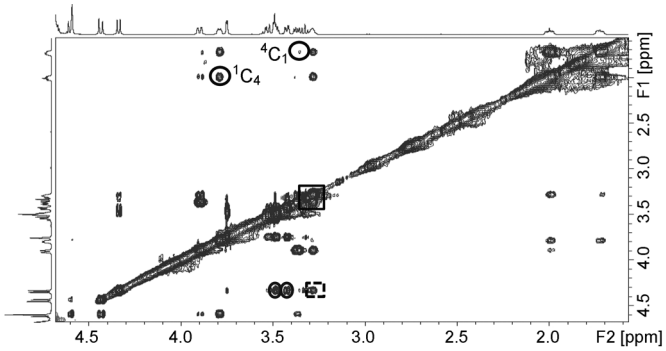

Figure 6. TR-NOESY of compound **2** (20 mM phosphate buffer with 1 mM $MgCl_2$ at pH 7.2 at 298 K). Circles highlight the key NOEs that define the different chair conformations of the aglycone, whereas the squares refer to the characteristic NOEs that define the conformations around the thioglycosydic torsion angles. Circles with legends refer to the aglyconic moiety, whereas the circles without legends refer to the Gal residue, which always presents a $^4C_1$ chair conformation. Lined squares indicate the presence of *anti*-$\Phi_{^4C_1}$/*syn*-$\Psi_{^4C_1}$ forms, whereas complete squares strongly suggest the existence of *syn*-$\Phi_{^1C_4}$/*syn*-$\Psi_{^1C_4}$ bound geometries. Protein/ligand molar ratio was 1:30.

selection process takes place during the recognition event. Now, the enzyme preferentially binds two conformers of compound **2** of the complex ensemble, which already existed in equilibrium in the free state.

If we consider both cases in a global manner, it seems that there is a direct correlation between the recognized Φ/Ψ conformer and the shape of the bound pentopyranose ring. The *anti*-Φ/*syn*-Ψ conformer correlates with a $^4C_1$ chair, whereas the *syn*-Φ/*syn*-Ψ geometry is associated with the alternative $^1C_4$ form. Interestingly, the major conformation in the free state, with $^4C_1$ chair and *syn*-Φ/*syn*-Ψ, is not recognized, in either case. Thus, the enzyme distorts the free state conformation, either by rotation of Φ (*syn*-$\Phi \rightarrow$*anti*-Φ) or at the aglycone, thus changing from $^4C_1$ to the $^1C_4$ chair.

Docking studies: Once the NMR spectroscopic results had been analyzed, a molecular docking protocol was used to provide plausible three-dimensional structures of the complexes, compatible with the experimental data. The docking studies were performed using Glide (Schrödinger), with the standard parameters (standard precision) procedure and without any constraints. In all cases, the docking protocol focused only on the carbohydrate recognition site, as deduced from the published X-ray crystal structure of *E. coli* β-galactosidase complexed with a substrate analogue, 2-fluoro-2-deoxy-D-lactose (PDB access code 1JYY). For both compounds, **1** and **2**, two starting geometries were chosen with the pentopyranose ring in either $^4C_1$ or $^1C_4$ chair conforma-

tion. The minimized geometries for Φ and Ψ were deduced by NMR spectroscopy, with either *syn* or *anti* dispositions being selected as the initial structures. The docking solutions were clustered depending on the geometry of the thioglycosidic linkage (Φ,Ψ) and that of the pentopyranose chair. Two essential features define each conformer, as described above: the chair conformation of the aglyconic moiety and the glycosidic torsion angles, Φ and Ψ. The geometry of the pyranose ring of the aglycone was readily deduced by monitoring the distance between H3b and H5b of the deoxypyranose (approximately 2.5 Å in the $^4C_1$ conformation). Deviation from this distance to higher values should account for the existence of the alternative $^1C_4$ chair conformation (4.1 Å in $^1C_4$ conformation). Similarly, the existence of *syn*-Φ/*syn*-Ψ geometries around the thioglycosidic torsion angles might be assessed by the distance between Gal H1′ and the pentopyranose H4 (<2.5 Å in this conformation). The shifting to *anti* geometries produces longer distances between these two key hydrogen atoms. Indeed, the 3D population histogram displayed in Figure 7 predicts the existence of three major binding modes of compound **2** to this enzyme: a minor *syn*-$\Phi_{^4C_1}$/*syn*-$\Psi_{^4C_1}$ population, followed by the *syn*-$\Phi_{^1C_4}$/*syn*-$\Psi_{^1C_4}$, and then the most populated conformer, *anti*-$\Phi_{^4C_1}$/*syn*-$\Psi_{^4C_1}$. These predictions are in agreement with the NMR spectroscopic experimental data, which suggested the existence of the *syn*-$\Phi_{^1C_4}$/*syn*-$\Psi_{^1C_4}$ and the *anti*-$\Phi_{^4C_1}$/*syn*-$\Psi_{^4C_1}$ geometries for the bound states. The essential geometric features that define these conformations will be discussed in the next section.

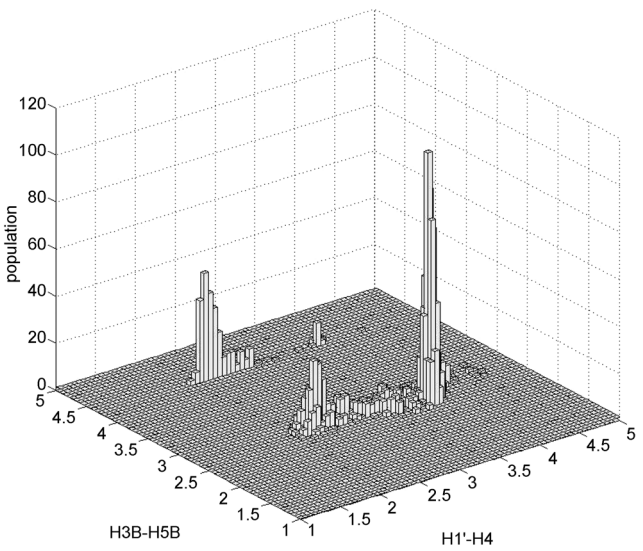

Figure 7. Bound conformers of thiodisaccharide **2** to *E. coli* β-galactosidase according to the docking protocol performed by employing Glide (Schrödinger). On the left-hand side, the axis defines the distance between H3b and H5b of the deoxyarabinose ring in the $^4C_1$ conformation (approximately 2.5 Å) and $^1C_4$ (4.1 Å) conformations. On the right-hand side, the axis defines the distance between Gal H1′ and the pentose H4 hydrogen. Distances around 2.3 Å account for *syn*-Φ/*syn*-Ψ geometries, whereas distances above 3.5 Å account for *anti*-type geometries for this glycosidic linkage. Thus, three major clusters are predicted by the calculations.

Molecular dynamics (MD) simulations: Since the docking process was performed by considering the protein as a rigid entity, the "best" docked structures (in terms of score functions) and those which agreed with the experimental NMR spectroscopic data, were then subjected to MD simulations to test their conformational stability. Therefore, the two representative docking solutions, one for each of the two docking clusters (*syn*-$\Phi_{^1C_4}$/*syn*-$\Psi_{^1C_4}$ and the *anti*-$\Phi_{^4C_1}$/*syn*-$\Psi_{^4C_1}$ geometries), were optimized and subjected to 10 ns unrestrained MD runs. During the simulations, the protein structures were stable, and the bound ligands remained at the binding site without diffusing into the solvent. In addition, no chair-to-chair or chair-to-boat interconversions were observed for the six-membered rings at either the glycon or aglyconic moieties.

In all cases, for both conformers of compound **1** and both conformers of compound **2**, the thioglycosidic torsion angles were fairly stable during the MD simulations, in agreement with the experimental NMR spectroscopic data (Figure 8)

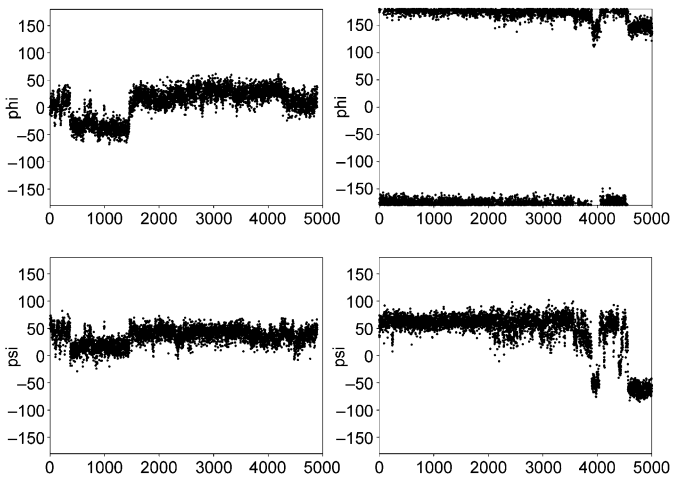

Figure 8. Trajectory of the Φ (top) and Ψ (bottom) torsion angles of **2** during the MD runs (5000 steps of two picoseconds each). Left: MD starting with the $^1C_4$ conformation for the pentose. The angle Φ is fixed in the *syn* geometry throughout the simulation. Right: MD starting with the $^4C_1$ conformation for the pentose. The *anti*-Φ conformer is fixed throughout the simulation.

and with a very major orientation for Φ, depending on the initial structure, which was kept during the MD trajectory. As mentioned above, at the binding site, the recognized Φ/Ψ conformer and the shape of the bound pentopyranose ring are correlated. This fact is also observed in the MD study. With regard to the Ψ angle, certain fluctuations were observed, but always within the *syn*-Ψ region. Nevertheless, depending on the *syn* or *anti* orientation of Φ, on the $^1C_4$ or $^4C_1$ geometry of the algycon, and on the change from positive to negative Ψ torsion values, the presentation of the surfaces of the Gal and aglyconic moieties that interact with the enzyme was different. Geometric parameters, such as interatomic distances and torsion angles, were monitored during the MD run to verify the stability and stabilizing fac-

tors in the formed complexes. Substantial differences were found in the orientation and intermolecular interactions inside the β-galactosidase binding site. For monitoring CH–π interactions, an essential and universal feature for galactose-binding protein complexes, side-chain centroids were defined for the key tryptophan residues (Trp^{568} and Trp^{999}). The distance between the Gal unit and Trp^{568} centroid was maintained constant for all simulations, as the Gal/Trp^{568} stacking is an intrinsic feature of the interaction of Gal-containing molecules with this β-galactosidase. In fact, during the MD run, the carbohydrate–aromatic stacking between the Gal unit and Trp^{568} was very well defined.

In the complexes of ligands **1** and **2** with the enzyme, several hydrogen bonds maintain the Gal moiety bound into the active site of the enzyme. Some known interactions are Gal O2/Glu^{461}, Gal O3/Glu^{537}, Gal O4/Asp^{201}, Gal O6/His^{560}, Gal O6/Asn^{604}, and Gal O6/Asp^{201}. Additional transient interactions between Gal OH-3 and OH-2 with Met^{502} and Tyr^{503} could be also observed with both *syn*-$\Phi_{^1C_4}$/*syn*-$\Psi_{^1C_4}$ (Figure 9A and C) and the *anti*-$\Phi_{^4C_1}$/*syn*-$\Psi_{^4C_1}$ (Figure 9B and D) geometries. As expected, the presentation of the aglycone in the complex depends on the glycosidic torsion angles and on the shape of the pentopyranose ring. In fact, for thiodisaccharides **1** and **2**, stacking interactions were observed for H3a, H4, and H5a in the aglycone $^1C_4$ conformation with Trp^{999}, which also interacts with Gal H1′. On the contrary, no stacking was observed for the same protons of the aglycone in its *anti*-$\Phi_{^4C_1}$/*syn*-$\Psi_{^4C_1}$ geometry. Nevertheless, in the case of **2**, the pentose ring in the $^1C_4$ conformation showed a hydrogen bond between its equatorially oriented OH-2 with the side chain of Asn^{102}, whereas for the alternative *anti*-$\Phi_{^4C_1}$/*syn*-$\Psi_{^4C_1}$ conformation, hydrogen bonding took place between the now axial OH-2 with Asn^{102} and the backbone NH of Val^{103}, as well as between Asn^{102} and the anomeric oxygen. Thus, the presentation of the aglycone is dramatically different in both docked complexes. In the *anti*-$\Phi_{^4C_1}$/*syn*-$\Psi_{^4C_1}$ conformer, the aglycone resembles the orientation for a departing leaving group at the end of the enzymatic process. On the other hand, compound **2** in the *syn*-$\Phi_{^1C_4}$/*syn*-$\Psi_{^1C_4}$ conformer (Figure 9C) is nicely accommodated without any significant perturbation of the enzyme binding site. The position of the aromatic group attached to the reducing end was also monitored. For the $^1C_4$ conformer of the pentopyranose, aromatic–aromatic interactions between the benzyl group and Phe^{512} were temporarily observed during the MD trajectory (Figure S7A in the Supporting Information). Alternatively, for the $^4C_1$ chair, the aromatic moiety established transient cation–π interactions with the guanidinium group of Arg^{800} (Figure S10B in the Supporting Information). All these interactions might explain the coexistence of two bound forms at the binding site of *E. coli* β-galactosidase, even when one of them basically does not exist in solution in the unbound state. On the contrary, compound **2** does not bind to the enzyme in the regular (for lactose) *syn*-$\Phi_{^4C_1}$/*syn*-$\Psi_{^4C_1}$ conformation. The explanation for this fact is probably again related to stacking interactions. In this *syn*-$\Phi_{^4C_1}$/*syn*-$\Psi_{^4C_1}$ conformer, the aglycone OH-2 in the $^4C_1$ chair is oriented towards the indol aromatic ring of Trp^{999}, thereby producing an OH-2–π interaction, which has been shown to be energetically disfavored in a variety of carbohydrate–protein complexes studied in aqueous solution.[14] This is probably the reason for the conformational change observed for this molecule upon binding to this enzyme.

Analogous interactions were observed for the complex of **1** with β-galactosidase. In the bound conformers, the docking/MD analyses suggest the already-mentioned interactions of

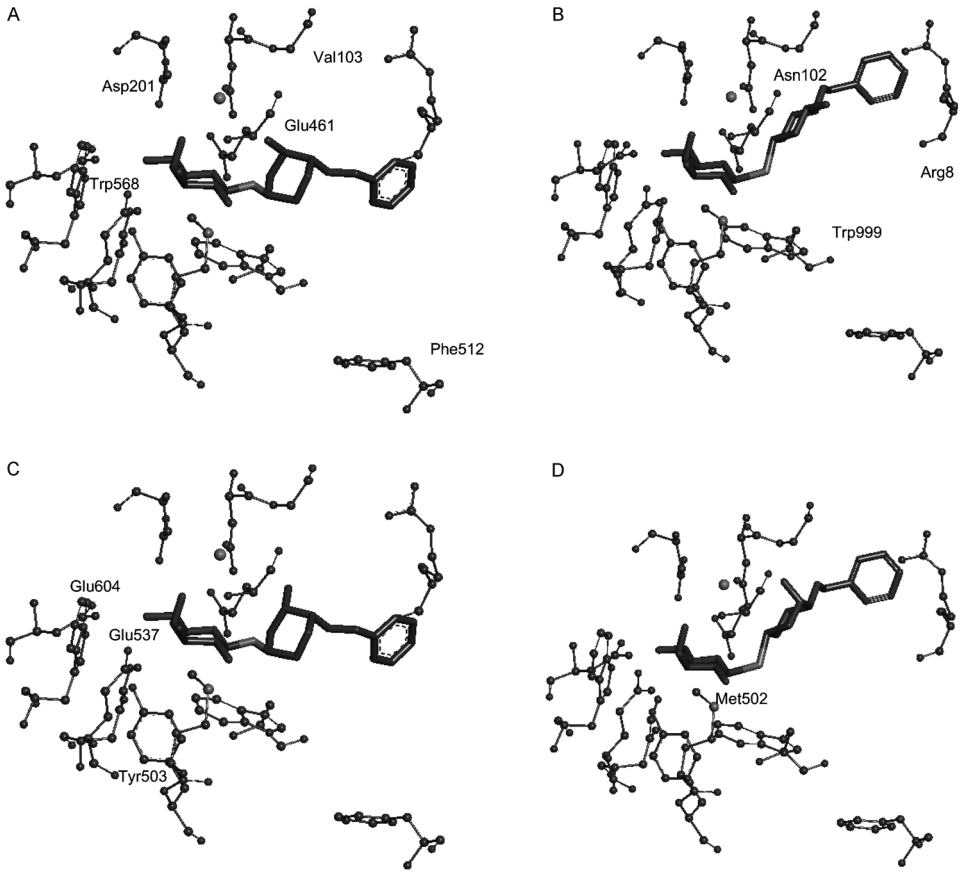

Figure 9. Representation of the docked structures of **1** and **2** to the enzyme. The key amino acids that surround the ligand are shown: A) Ligand **1** *syn*-$\Phi_{^1C_4}$/*syn*-$\Psi_{^1C_4}$, B) ligand **1** *anti*-$\Phi_{^4C_1}$/*syn*-$\Psi_{^4C_1}$, C) ligand **2** *syn*-$\Phi_{^1C_4}$/*syn*-$\Psi_{^1C_4}$, D) ligand **2** *anti*-$\Phi_{^4C_1}$/*syn*-$\Psi_{^4C_1}$.

the Gal moiety, which keep this part of the molecule fixed in its starting conformation. For the pentopyranose ring, the $syn\text{-}\Phi_{^1C_4}/syn\text{-}\Psi_{^1C_4}$ form, in addition to the stacking interactions that involve H3a, H4, and H5a, shows the hydrogen bonding of axial OH-2 to the side chain of Asn^{102}. In the alternative $anti\text{-}\Phi_{^4C_1}/syn\text{-}\Psi_{^4C_1}$ conformer, the equatorial orientation of OH-2 of the pentose precludes the hydrogen-bond interaction to Asn^{102}. Thus, in this complex, Asn^{102} exhibits only hydrogen bonding to the endocyclic pentose oxygen. In this arrangement, the number of interactions of the pentose moiety of **1** with the enzyme is smaller than for **2**, which is in agreement with the weaker inhibition ability of **1** with respect to **2**. If we also take into account the drastic variation of conformation that takes place in **1**, when passing from the free to the bound state, the gain in free energy for binding **1** should be higher than that for binding **2**. With regard to the lack of proper binding to the enzyme of the major $syn\text{-}\Phi_{^4C_1}/syn\text{-}\Psi_{^4C_1}$ conformation present in solution for **1**, it seems that, according to the docking studies, this conformer could be adapted to the enzyme binding site without major problems. No involvement of the pentopyranose moiety in hydrogen-bonding interactions would take place, according to the obtained docking pose, with respect to those observed in the alternative conformations. This explanation could account for the experimental observations. Nevertheless, the distinction between the STD data between **1** and **2** suggested that the binding mode of both **1** and **2** could be different, and that **1** could target a different site. Indeed, the enzymatic experiments performed for **1** suggested that the inhibition mode of **1** belongs to the noncompetitive type. Given the size of the enzyme, many patches could accommodate the structure of **1**, thereby producing the weak inhibition observed.

Conclusion

Two novel thiodisaccharides have shown rather distinct inhibitory activity against *E. coli* β-galactosidase. Compound **1** has an inhibition constant of 800 μM, whereas K_i is 32 μM for its epimer compound, **2**. Thus, despite the existence of a mere change in the stereochemistry at a remote stereogenic center at the aglycone, there is a 25-fold difference in the inhibition constant. Interestingly, both molecules display a rather different conformational behavior in the free state, whereas the NMR spectroscopic data in the bound state demonstrate the existence of conformation selection processes upon binding to *E. coli* β-galactosidase. There are two bound conformations, the $anti\text{-}\Phi/syn\text{-}\Psi$ with a $^4C_1$ chair for the pentopyranose ring, and the $syn\text{-}\Phi/syn\text{-}\Psi$, with the alternative $^1C_4$ chair. Compound **2**, the more potent inhibitor, preferably adopts the bound conformation with $^1C_4$ chair. In contrast, **1** adopts both bound geometries in a similar ratio. Interestingly, the NMR spectroscopic data show that the ground state $syn\text{-}\Phi/syn\text{-}\Psi$ conformer, typical for *O*-glycoside lactose analogues, is not bound. In both cases, the enzyme selects unusual conformations of the inhibitor, either at the glycosidic bond (*anti*-Φ) or at the aglyconic moiety ($^1C_4$ chair). Thus, it seems that the enzyme prefers to bind to distorted forms of the ligand. It is tempting to speculate that this could be a trick that the enzyme employs to minimize the energy required for catalysis in this type of substrate. In a series of recent papers, Rovira et al., Davies et al., and others[15] have described that pyranoses adopt distorted conformations in several complexes with glycosidases. We report here a unique case of binding of a ligand in a distorted geometry that involves the aglyconic moiety instead of that of the galactose that undergoes glycosidic bond breaking during the enzymatic reaction. The 25-fold difference in the inhibition ability suggests that a new generation of inhibitors might be designed by modifying the aglycone at selected positions, even if distant from the reaction site. The adaptability of the ligand to the enzyme binding site is also a prerequisite for this approach to be successful.

Experimental Section

Compounds and enzymatic assays: The synthesis of these compounds has been already described in detail.[11] The enzymatic assays were performed with β-galactosidase from *Escherichia coli*; this same enzyme has been utilized in the reported study. The enzyme was purchased from Sigma–Aldrich and it was necessary to eliminate Tris-HCl buffer to run the experiments. Vivaspin 6 10000 molecular-weight cutoff (MWCO) polyethersulfone (PES) filters provided the cleanup and buffer exchange to 20 mM phosphate buffer and 1 mM $MgCl_2$ (pH 7.2).

Molecular mechanics calculations: Potential-energy maps for the thioglycosides[16] shown in the Supporting Information were calculated by employing the Coordinate Scan tool from the Maestro suite of programs.[17] The dihedral angles Φ and Ψ around the linkages between the nonreducing galactose residue and the aglyconic deoxypentose unit were calculated with the AMBER* force field. The calculation method used the PRCG protocol by employing an energy-minimization process. The maps were employed to visualize the possible local minima regions, depending on the shape of the pyranose ring. Therefore, independent potential-energy maps were computed for both the $^1C_4$ and $^4C_1$ shapes. The geometries of the more stable structures within the local minima regions were employed to interpret the NMR spectroscopic data. Thus, the actual relative energies estimated by the molecular mechanics calculations were not considered for the interpretation of the data.

Docking analysis: All docking studies were performed by using Glide docking software (version 5.5)[18] and the standard parameters within the standard precision procedure without any constraints. The starting coordinates for the enzyme were obtained from the Protein Data Bank (www.rcsb.org), PDB code 1JYY (2.7 Å resolution).[1b] This structure was chosen because it is a complex of the enzyme with 2-F-lactose disaccharide. Prior to docking studies, the structure was prepared with the Wizard program (Maestro package); ions and water molecules that are not implied in the recognition were removed, and polar hydrogen atoms were added. Protonation of histidine residues was checked manually, and the ligand was removed. After treatments of protein (Protein Preparation Wizard) and ligand (LigPrep), the docking analysis was performed by Glide from the Schrodinger pack. The grid box was defined as a cube 25 Å on a side centered at the enzymatic pocket. All structures from LigPrep used on docking analysis and Glide were set to obtain a considerable population of poses that can be grouped into families.

Molecular dynamics: The AMBER force field with the GLYCAM[19] and ff99 parameter sets were employed for the description of the β-galactosidase-inhibitor complexes. All molecular dynamics simulations were carried out using the Sander module in the AMBER 10.[20] Thirty-two Na^+ counterions were added to neutralize the system. Each system was then

solvated by using TIP3P waters[21] in a cubic box with at least 8 Å distance around the complex. The Shake algorithm was applied to all hydrogen-containing bonds,[22] and a 1 fs integration step was used. The simulation used periodic boundary conditions, and the electrostatic interactions were represented by using the smooth particle mesh Ewald method[23] with a grid spacing of 1 Å. Each system was gently annealed from 100 to 300 K over a period of 25 ps. The systems were then maintained at a temperature of 300 K for 50 ps with a solute restraint and progressive energy minimizations, gradually releasing the restraints of the solute, followed by a 20 ps heating phase from 100 to 300 K, when restraints were removed. Finally, the production simulations for each system lasted 10 ns and were also continued in the isothermal–isobaric ensemble. Coordinate trajectories were recorded each 2 ps throughout all equilibration and production runs, which yielded an ensemble of 1500 structures of each complex for further analysis.

MD trajectories were analyzed by using a combination of the AMBER and VMD[24] packages. Overall root-mean-square deviation (RMSD) variations were computed with ptraj (AMBER) after superimposition of the C^{α}, C, and N atoms (protein backbone) of β-galactosidase. The evolution of hydrogen bonds between the inhibitor and amino acids and the water during the 10 ns simulation were identified with ptraj (an Amber utility, cutoff = 4 A). The dihedral Φ/Ψ torsion angles were determined during the simulation time. Also, the carbohydrate orientation at the binding site was established by measuring the significant distances between the sugar units and the key amino acids.

NMR spectroscopy: The NMR spectroscopic experiments were recorded at 298 K in D_2O, using a Bruker AV600 Spectrometer. Enzyme samples were recorded in sodium phosphate buffer (20 mM, pH 7.2) with 1 mM $MgCl_2$. Spectra were obtained with standard sequences from TOPSPIN software package. Due to residual water molecules, a 2D sequence was required to suppress an HDO signal from spectra to clarify the information. For the NOESY and TR-NOESY, the sequence noesygpph19 was employed; for selective NOE spectra, the selnogp; and for the saturation transfer difference (STD), the std2. NOESY experiments in free states were set with mixing times of 200 and 500 ms, and TR-NOESY with mixing times of 80, 100, 150, and 200 ms. Transfer NOE spectra were performed with a protein/ligand molar ratio of 1:10 and no T2 filter or short-spin lock pulse SL was necessary to remove the background of the protein because the huge size of *E. coli* β-galactosidase determines a practically flat baseline (116.3 kDa for the tetramer). STD-NMR experiments were performed with a 1:100 protein/ligand molar ratio. An off-resonance frequency of 100 ppm and an on-resonance frequency of −0.5 ppm (protein aliphatic signal region) were applied. Saturation curves were built with STD values measured according to increasing saturation times (0.5, 1, 1.5, 2, and 2.5 s). Afterwards, the relative saturation percentages were normalized with respect to the proton with the strongest response.

Acknowledgements

The group from Madrid thanks MINECO (grants CTQ2009-08536 and CTQ2012-32025), the Comunidad de Madrid (MHit project), as well as the BM1003 and CM1102 COST actions, and the GlycoHit and GlycoPharm projects, funded by the European Union. The group from Buenos Aires thanks the University of Buenos Aires, the National Research Council of República Argentina (CONICET), and the National Agency for Promotion of Science and Technology of Argentina (ANPCyT). O.V. and M.L.U. are research members of CONICET.

[1] a) B. Henrissat, A. Bairoch, *Biochem. J.* **1993**, *293*, 781–788; b) D. H. Juers, T. D. Heightman, A. Vasella, J. D. McCarter, L. Mackenzie, S. G. Withers, B. W. Matthews, *Biochemistry* **2001**, *40*, 14781–14794; c) R. H. Jacobson, X. J. Zhang, R. F. DuBose, B. W. Matthews, *Nature* **1994**, *369*, 761–766; d) M. L. Dugdale, M. L. Vance, R. W. Wheatley, M. R. Driedger, A. Nibber, A. Tran, R. E. Huber, *Biochem. Cell Biol.* **2010**, *88*, 969–979.

[2] a) J. F. Espinosa, F. J. Cañada, J. L. Asensio, M. Martin-Pastor, H. Dietrich, M. Martín-Lomas, R. R. Schmidt, J. Jiménez-Barbero, *J. Am. Chem. Soc.* **1996**, *118*, 10862–10871; b) J. L. Asensio, J. F. Espinosa, H. Dietrich, F. J. Cañada, R. R. Schmidt, M. Martín-Lomas, S. André, H. J. Gabius, J. Jiménez-Barbero, *J. Am. Chem. Soc.* **1999**, *121*, 8995–9000; c) G. J. Davies, A. Planas, C. Rovira, *Acc. Chem. Res.* **2012**, *45*, 308–316.

[3] a) "Combining Computational Chemistry and Crystallography for a Better Understanding of the Structure of Cellulose":A. D. French in *Advances in Carbohydrate Chemistry and Biochemistry Vol. 67* (Ed.: H. Derek), Academic Press, **2012**, pp. 19–93; b) G. P. Johnson, L. Petersen, A. D. French, P. J. Reilly, *Carbohydr. Res.* **2009**, *344*, 2157–2166.

[4] A. Vasella, G. J. Davies, M. Böhm, *Curr. Opin. Chem. Biol.* **2002**, *6*, 619–629.

[5] a) B. P. Rempel, S. G. Withers, *Glycobiology* **2008**, *18*, 570–586; b) J. Pabba, A. Vasella, *Helv. Chim. Acta* **2006**, *89*, 2006–2019.

[6] a) M. Ring, D. E. Bader, R. E. Huber, *Biochem. Biophys. Res. Commun.* **1988**, *152*, 1050–1055; b) D. E. Bader, M. Ring, R. E. Huber, *Biochem. Biophys. Res. Commun.* **1988**, *153*, 301–306.

[7] B. W. Matthews, *C. R. Biol.* **2005**, *328*, 549–556.

[8] V. Spiwok, P. Lipovová, T. Skálová, E. Buchtelová, J. Hasek, B. Králová, *Carbohydr. Res.* **2004**, *339*, 2275–2280.

[9] A. T. Hadfield, D. J. Harvey, D. B. Archer, D. A. MacKenzie, D. J. Jeenes, S. E. Radford, G. Lowe, C. M. Dobson, L. N. Johnson, *J. Mol. Biol.* **1994**, *243*, 856–872.

[10] a) A. García-Herrero, E. Montero, J. L. Muñoz, J. F. Espinosa, A. Vián, J. L. García, J. L. Asensio, F. J. Cañada, J. Jiménez-Barbero, *J. Am. Chem. Soc.* **2002**, *124*, 4804–4810; b) J. F. Espinosa, E. Montero, A. Vian, J. L. García, H. Dietrich, R. R. Schmidt, M. Martín-Lomas, A. Imberty, F. J. Cañada, J. Jiménez-Barbero, *J. Am. Chem. Soc.* **1998**, *120*, 1309–1318.

[11] A. J. Cagnoni, M. L. Uhrig, O. Varela, *Bioorg. Med. Chem.* **2009**, *17*, 6203–6212.

[12] M. Mayer, B. Meyer, *Angew. Chem.* **1999**, *111*, 1902–1906; *Angew. Chem. Int. Ed.* **1999**, *38*, 1784–1788.

[13] G. M. Clore, A. M. Gronenborn, *J. Magn. Reson.* **1983**, *53*, 423–442.

[14] S. Vandenbussche, D. Díaz, M. C. Fernández-Alonso, W. Pan, S. P. Vincent, G. Cuevas, F. J. Cañada, J. Jiménez-Barbero, K. Bartik, *Chem. Eur. J.* **2008**, *14*, 7570–7578.

[15] a) X. Biarnés, A. Ardèvol, A. Planas, C. Rovira, A. Laio, M. Parrinello, *J. Am. Chem. Soc.* **2007**, *129*, 10686–10693; b) A. Lammerts van Bueren, A. Ardèvol, J. Fayers-Kerr, B. Luo, Y. Zhang, M. Sollogoub, Y. Blériot, C. Rovira, G. J. Davies, *J. Am. Chem. Soc.* **2010**, *132*, 1804–1806; c) T. M. Gloster, G. J. Davies, *Org. Biomol. Chem.* **2010**, *8*, 305–320.

[16] F. Strino, J.-H. Lii, H.-J. Gabius, P.-G. Nyholm, *J. Comput-Aided Mol. Des.* **2009**, *23*, 845–852.

[17] Maestro, a powerful all-purpose molecular modeling environment, version 8.5, Schödinger, LLC, New York, NY, **2008**.

[18] Glide, version 5.5, Schrödinger, Inc., New York, NY, **2009**.

[19] K. N. Kirschner, A. B. Yongye, S. M. Tschampel, J. Gonzalez-Outeirino, C. R. Daniels, B. L. Foley, R. J. Woods, *J. Comput. Chem.* **2008**, *29*, 622–655.

[20] D. A. Case, T. E. Cheatham, T. Darden, H. Gohlke, R. Luo, K. M. Merz, A. Onufriev, C. Simmerling, B. Wang, R. J. Woods, *J. Comput. Chem.* **2005**, *26*, 1668–1688.

[21] W. L. Jorgensen, J. Chandrasekhar, J. D. Madura, R. W. Impey, M. L. Klein, *J. Chem. Phys.* **1983**, *79*, 926–935.

[22] J.-P. Ryckaert, G. Ciccotti, H. J. C. Berendsen, *J. Comput. Phys.* **1977**, *23*, 327–341.

[23] D. M. York, T. A. Darden, L. G. Pedersen, *J. Chem. Phys.* **1993**, *99*, 8345–8348.

[24] W. Humphrey, A. Dalke, K. Schulten, *J. Mol. Graphics* **1996**, *14*, 33–38.

Received: October 15, 2012
Published online: February 19, 2013

